EUROPEAN ORGANIZATION FOR NUCLEAR RESEARCH

CERN–EP/98–170

27 October 1998

Search for lightest neutralino and stau pair production in light gravitino scenarios with stau NLSP

DELPHI Collaboration

Abstract

Promptly decaying lightest neutralinos and long-lived staus are searched for in the context of light gravitino scenarios. It is assumed that the stau is the next to lightest supersymmetric particle (NLSP) and that the lightest neutralino is the next to NLSP (NNLSP). Data collected with the Delphi detector at centre-of-mass energies from 161 to 183 GeV are analysed. No evidence of the production of these particles is found. Hence, lower mass limits for both kinds of particles are set at 95% C.L.. The mass of gaugino-like neutralinos is found to be greater than 71.5 GeV/c^2. In the search for long-lived stau, masses less than 70.0 to 77.5 GeV/c^2 are excluded for gravitino masses from 10 to 150 eV/c^2. Combining this search with the searches for stable heavy leptons and Minimal Supersymmetric Standard Model staus a lower limit of 68.5 GeV/c^2 may be set for the stau mass independent of the mass of the gravitino.

(Submitted to E. Phys. J. C)

P.Abreu[21], W.Adam[50], T.Adye[36], P.Adzic[11], T.Aldeweireld[2], G.D.Alekseev[16], R.Alemany[49], T.Allmendinger[17], P.P.Allport[22], S.Almehed[24], U.Amaldi[9], S.Amato[47], E.G.Anassontzis[3], P.Andersson[44], A.Andreazza[9], S.Andringa[21], P.Antilogus[25], W-D.Apel[17], Y.Arnoud[14], B.Åsman[44], J-E.Augustin[25], A.Augustinus[9], P.Baillon[9], P.Bambade[19], F.Barao[21], G.Barbiellini[46], R.Barbier[25], D.Y.Bardin[16], G.Barker[9], A.Baroncelli[38], M.Battaglia[15], M.Baubillier[23], K-H.Becks[52], M.Begalli[6], P.Beilliere[8], Yu.Belokopytov[9,53], K.Belous[42], A.C.Benvenuti[5], C.Berat[14], M.Berggren[25], D.Bertini[25], D.Bertrand[2], M.Besancon[39], F.Bianchi[45], M.Bigi[45], M.S.Bilenky[16], M-A.Bizouard[19], D.Bloch[10], H.M.Blom[30], M.Bonesini[27], W.Bonivento[27], M.Boonekamp[39], P.S.L.Booth[22], A.W.Borgland[4], G.Borisov[19], C.Bosio[41], O.Botner[48], E.Boudinov[30], B.Bouquet[19], C.Bourdarios[19], T.J.V.Bowcock[22], I.Boyko[16], I.Bozovic[11], M.Bozzo[13], P.Branchini[38], T.Brenke[52], R.A.Brenner[48], P.Bruckman[18], J-M.Brunet[8], L.Bugge[32], T.Buran[32], T.Burgsmueller[52], P.Buschmann[52], S.Cabrera[49], M.Caccia[27], M.Calvi[27], A.J.Camacho Rozas[40], T.Camporesi[9], V.Canale[37], F.Carena[9], L.Carroll[22], C.Caso[13], M.V.Castillo Gimenez[49], A.Cattai[9], F.R.Cavallo[5], V.Chabaud[9], M.Chapkin[42], Ph.Charpentier[9], L.Chaussard[25], P.Checchia[35], G.A.Chelkov[16], R.Chierici[45], P.Chliapnikov[42], P.Chochula[7], V.Chorowicz[25], J.Chudoba[29], P.Collins[9], M.Colomer[49], R.Contri[13], E.Cortina[49], G.Cosme[19], F.Cossutti[39], J-H.Cowell[22], H.B.Crawley[1], D.Crennell[36], G.Crosetti[13], J.Cuevas Maestro[33], S.Czellar[15], G.Damgaard[28], M.Davenport[9], W.Da Silva[23], A.Deghorain[2], G.Della Ricca[46], P.Delpierre[26], N.Demaria[9], A.De Angelis[9], W.De Boer[17], S.De Brabandere[2], C.De Clercq[2], B.De Lotto[46], A.De Min[35], L.De Paula[47], H.Dijkstra[9], L.Di Ciaccio[37], J.Dolbeau[8], K.Doroba[51], M.Dracos[10], J.Drees[52], M.Dris[31], A.Duperrin[25], J-D.Durand[25,9], G.Eigen[4], T.Ekelof[48], G.Ekspong[44], M.Ellert[48], M.Elsing[9], J-P.Engel[10], B.Erzen[43], M.Espirito Santo[21], E.Falk[24], G.Fanourakis[11], D.Fassouliotis[11], J.Fayot[23], M.Feindt[17], A.Fenyuk[42], P.Ferrari[27], A.Ferrer[49], E.Ferrer-Ribas[19], S.Fichet[23], A.Firestone[1], P.-A.Fischer[9], U.Flagmeyer[52], H.Foeth[9], E.Fokitis[31], F.Fontanelli[13], B.Franek[36], A.G.Frodesen[4], R.Fruhwirth[50], F.Fulda-Quenzer[19], J.Fuster[49], A.Galloni[22], D.Gamba[45], S.Gamblin[19], M.Gandelman[47], C.Garcia[49], J.Garcia[40], C.Gaspar[9], M.Gaspar[47], U.Gasparini[35], Ph.Gavillet[9], E.N.Gazis[31], D.Gele[10], N.Ghodbane[25], I.Gil[49], F.Glege[52], R.Gokieli[51], B.Golob[43], G.Gomez-Ceballos[40], P.Goncalves[21], I.Gonzalez Caballero[40], G.Gopal[36], L.Gorn[1,54], M.Gorski[51], Yu.Gouz[42], V.Gracco[13], J.Grahl[1], E.Graziani[38], C.Green[22], H-J.Grimm[17], P.Gris[39], K.Grzelak[51], M.Gunther[48], J.Guy[36], F.Hahn[9], S.Hahn[52], S.Haider[9], A.Hallgren[48], K.Hamacher[52], F.J.Harris[34], V.Hedberg[24], S.Heising[17], J.J.Hernandez[49], P.Herquet[2], H.Herr[9], T.L.Hessing[34], J.-M.Heuser[52], E.Higon[49], S-O.Holmgren[44], P.J.Holt[34], D.Holthuizen[30], S.Hoorelbeke[2], M.Houlden[22], J.Hrubec[50], K.Huet[2], K.Hultqvist[44], J.N.Jackson[22], R.Jacobsson[9], P.Jalocha[9], R.Janik[7], Ch.Jarlskog[24], G.Jarlskog[24], P.Jarry[39], B.Jean-Marie[19], E.K.Johansson[44], P.Jonsson[24], C.Joram[9], P.Juillot[10], F.Kapusta[23], K.Karafasoulis[11], S.Katsanevas[25], E.C.Katsoufis[31], R.Keranen[17], B.P.Kersevan[43], B.A.Khomenko[16], N.N.Khovanski[16], A.Kiiskinen[15], B.King[22], N.J.Kjaer[30], O.Klapp[52], H.Klein[9], P.Kluit[30], P.Kokkinias[11], M.Koratzinos[9], V.Kostioukhine[42], C.Kourkoumelis[3], O.Kouznetsov[16], M.Krammer[50], C.Kreuter[9], E.Kriznic[43], J.Krstic[11], Z.Krumstein[16], P.Kubinec[7], W.Kucewicz[18], K.Kurvinen[15], J.W.Lamsa[1], D.W.Lane[1], P.Langefeld[52], V.Lapin[42], J-P.Laugier[39], R.Lauhakangas[15], F.Ledroit[14], V.Lefebure[2], L.Leinonen[44], A.Leisos[11], R.Leitner[29], G.Lenzen[52], V.Lepeltier[19], T.Lesiak[18], M.Lethuillier[39], J.Libby[34], D.Liko[9], A.Lipniacka[44], I.Lippi[35], B.Loerstad[24], J.G.Loken[34], J.H.Lopes[47], J.M.Lopez[40], R.Lopez-Fernandez[14], D.Loukas[11], P.Lutz[39], L.Lyons[34], J.MacNaughton[50], J.R.Mahon[6], A.Maio[21], A.Malek[52], T.G.M.Malmgren[44], V.Malychev[16], F.Mandl[50], J.Marco[40], R.Marco[40], B.Marechal[47], M.Margoni[35], J-C.Marin[9], C.Mariotti[9], A.Markou[11], C.Martinez-Rivero[19], F.Martinez-Vidal[49], S.Marti i Garcia[22], J.Masik[29], N.Mastroyiannopoulos[11], F.Matorras[40], C.Matteuzzi[27], G.Matthiae[37], J.Mazik[29], F.Mazzucato[35], M.Mazzucato[35], M.Mc Cubbin[22], R.Mc Kay[1], R.Mc Nulty[9], G.Mc Pherson[22], C.Meroni[27], W.T.Meyer[1], E.Migliore[45], L.Mirabito[25], W.A.Mitaroff[50], U.Mjoernmark[24], T.Moa[44], R.Moeller[28], K.Moenig[9], M.R.Monge[13], X.Moreau[23], P.Morettini[13], G.Morton[34], U.Mueller[52], K.Muenich[52], M.Mulders[30], C.Mulet-Marquis[14], R.Muresan[24], W.J.Murray[36], B.Muryn[14,18], G.Myatt[34], T.Myklebust[32], F.Naraghi[14], F.L.Navarria[5], S.Navas[49], K.Nawrocki[51], P.Negri[27], N.Neufeld[9], N.Neumeister[50], R.Nicolaidou[14], B.S.Nielsen[28], M.Nikolenko[10,16], V.Nomokonov[15], A.Normand[22], A.Nygren[24], V.Obraztsov[42], A.G.Olshevski[16], A.Onofre[21], R.Orava[15], G.Orazi[10], K.Osterberg[15], A.Ouraou[39], M.Paganoni[27], S.Paiano[5], R.Pain[23], R.Paiva[21], J.Palacios[34], H.Palka[18], Th.D.Papadopoulou[31], K.Papageorgiou[11], L.Pape[9], C.Parkes[34], F.Parodi[13], U.Parzefall[22], A.Passeri[38], O.Passon[52], M.Pegoraro[35], L.Peralta[21], M.Pernicka[50], A.Perrotta[5], C.Petridou[46], A.Petrolini[13], H.T.Phillips[36], G.Piana[13], F.Pierre[39], M.Pimenta[21], E.Piotto[27], T.Podobnik[43], M.E.Pol[6], G.Polok[18], P.Poropat[46], V.Pozdniakov[16], P.Privitera[37], N.Pukhaeva[16], A.Pullia[27], D.Radojicic[34], S.Ragazzi[27], H.Rahmani[31], D.Rakoczy[50], P.N.Ratoff[20], A.L.Read[32], P.Rebecchi[9], N.G.Redaelli[27], M.Regler[50], D.Reid[9], R.Reinhardt[52], P.B.Renton[34], L.K.Resvanis[3], F.Richard[19], J.Ridky[12], G.Rinaudo[45], O.Rohne[32], A.Romero[45], P.Ronchese[35], E.I.Rosenberg[1], P.Rosinsky[7], P.Roudeau[19], T.Rovelli[5], V.Ruhlmann-Kleider[39], A.Ruiz[40], H.Saarikko[15], Y.Sacquin[39], A.Sadovsky[16], G.Sajot[14], J.Salt[49], D.Sampsonidis[11], M.Sannino[13], H.Schneider[17], Ph.Schwemling[23], U.Schwickerath[17], M.A.E.Schyns[52], F.Scuri[46], P.Seager[20], Y.Sedykh[16], A.M.Segar[34], R.Sekulin[36], R.C.Shellard[6], A.Sheridan[22], M.Siebel[52], R.Silvestre[39], L.Simard[39], F.Simonetto[35], A.N.Sisakian[16], T.B.Skaali[32], G.Smadja[25], N.Smirnov[42], O.Smirnova[24], G.R.Smith[36], A.Sopczak[17], R.Sosnowski[51], T.Spassov[21], E.Spiriti[38], P.Sponholz[52], S.Squarcia[13], D.Stampfer[50], C.Stanescu[38], S.Stanic[43], S.Stapnes[32], K.Stevenson[34], A.Stocchi[19], J.Strauss[50], R.Strub[10], B.Stugu[4], M.Szczekowski[51], M.Szeptycka[51], T.Tabarelli[27], F.Tegenfeldt[48], F.Terranova[27], J.Thomas[34], A.Tilquin[26], J.Timmermans[30], L.G.Tkatchev[16], S.Todorova[10], D.Z.Toet[30], A.Tomaradze[2], B.Tome[21], A.Tonazzo[27], L.Tortora[38], G.Transtromer[24], D.Treille[9], G.Tristram[8], C.Troncon[27], A.Tsirou[9],

M-L.Turluer[39], I.A.Tyapkin[16], S.Tzamarias[11], B.Ueberschaer[52], O.Ullaland[9], V.Uvarov[42], G.Valenti[5], E.Vallazza[46], G.W.Van Apeldoorn[30], P.Van Dam[30], J.Van Eldik[30], A.Van Lysebetten[2], I.Van Vulpen[30], N.Vassilopoulos[34], G.Vegni[27], L.Ventura[35], W.Venus[36], F.Verbeure[2], M.Verlato[35], L.S.Vertogradov[16], V.Verzi[37], D.Vilanova[39], L.Vitale[46], E.Vlasov[42], A.S.Vodopyanov[16], C.Vollmer[17], G.Voulgaris[3], V.Vrba[12], H.Wahlen[52], C.Walck[44], C.Weiser[17], D.Wicke[52], J.H.Wickens[2], G.R.Wilkinson[9], M.Winter[10], M.Witek[18], G.Wolf[9], J.Yi[1], O.Yushchenko[42], A.Zaitsev[42], A.Zalewska[18], P.Zalewski[51], D.Zavrtanik[43], E.Zevgolatakos[11], N.I.Zimin[16,24], G.C.Zucchelli[44], G.Zumerle[35]

[1] Department of Physics and Astronomy, Iowa State University, Ames IA 50011-3160, USA
[2] Physics Department, Univ. Instelling Antwerpen, Universiteitsplein 1, BE-2610 Wilrijk, Belgium
and IIHE, ULB-VUB, Pleinlaan 2, BE-1050 Brussels, Belgium
and Faculté des Sciences, Univ. de l'Etat Mons, Av. Maistriau 19, BE-7000 Mons, Belgium
[3] Physics Laboratory, University of Athens, Solonos Str. 104, GR-10680 Athens, Greece
[4] Department of Physics, University of Bergen, Allégaten 55, NO-5007 Bergen, Norway
[5] Dipartimento di Fisica, Università di Bologna and INFN, Via Irnerio 46, IT-40126 Bologna, Italy
[6] Centro Brasileiro de Pesquisas Físicas, rua Xavier Sigaud 150, BR-22290 Rio de Janeiro, Brazil
and Depto. de Física, Pont. Univ. Católica, C.P. 38071 BR-22453 Rio de Janeiro, Brazil
and Inst. de Física, Univ. Estadual do Rio de Janeiro, rua São Francisco Xavier 524, Rio de Janeiro, Brazil
[7] Comenius University, Faculty of Mathematics and Physics, Mlynska Dolina, SK-84215 Bratislava, Slovakia
[8] Collège de France, Lab. de Physique Corpusculaire, IN2P3-CNRS, FR-75231 Paris Cedex 05, France
[9] CERN, CH-1211 Geneva 23, Switzerland
[10] Institut de Recherches Subatomiques, IN2P3 - CNRS/ULP - BP20, FR-67037 Strasbourg Cedex, France
[11] Institute of Nuclear Physics, N.C.S.R. Demokritos, P.O. Box 60228, GR-15310 Athens, Greece
[12] FZU, Inst. of Phys. of the C.A.S. High Energy Physics Division, Na Slovance 2, CZ-180 40, Praha 8, Czech Republic
[13] Dipartimento di Fisica, Università di Genova and INFN, Via Dodecaneso 33, IT-16146 Genova, Italy
[14] Institut des Sciences Nucléaires, IN2P3-CNRS, Université de Grenoble 1, FR-38026 Grenoble Cedex, France
[15] Helsinki Institute of Physics, HIP, P.O. Box 9, FI-00014 Helsinki, Finland
[16] Joint Institute for Nuclear Research, Dubna, Head Post Office, P.O. Box 79, RU-101 000 Moscow, Russian Federation
[17] Institut für Experimentelle Kernphysik, Universität Karlsruhe, Postfach 6980, DE-76128 Karlsruhe, Germany
[18] Institute of Nuclear Physics and University of Mining and Metalurgy, Ul. Kawiory 26a, PL-30055 Krakow, Poland
[19] Université de Paris-Sud, Lab. de l'Accélérateur Linéaire, IN2P3-CNRS, Bât. 200, FR-91405 Orsay Cedex, France
[20] School of Physics and Chemistry, University of Lancaster, Lancaster LA1 4YB, UK
[21] LIP, IST, FCUL - Av. Elias Garcia, 14-1^{o}, PT-1000 Lisboa Codex, Portugal
[22] Department of Physics, University of Liverpool, P.O. Box 147, Liverpool L69 3BX, UK
[23] LPNHE, IN2P3-CNRS, Univ. Paris VI et VII, Tour 33 (RdC), 4 place Jussieu, FR-75252 Paris Cedex 05, France
[24] Department of Physics, University of Lund, Sölvegatan 14, SE-223 63 Lund, Sweden
[25] Université Claude Bernard de Lyon, IPNL, IN2P3-CNRS, FR-69622 Villeurbanne Cedex, France
[26] Univ. d'Aix - Marseille II - CPP, IN2P3-CNRS, FR-13288 Marseille Cedex 09, France
[27] Dipartimento di Fisica, Università di Milano and INFN, Via Celoria 16, IT-20133 Milan, Italy
[28] Niels Bohr Institute, Blegdamsvej 17, DK-2100 Copenhagen Ø, Denmark
[29] NC, Nuclear Centre of MFF, Charles University, Areal MFF, V Holesovickach 2, CZ-180 00, Praha 8, Czech Republic
[30] NIKHEF, Postbus 41882, NL-1009 DB Amsterdam, The Netherlands
[31] National Technical University, Physics Department, Zografou Campus, GR-15773 Athens, Greece
[32] Physics Department, University of Oslo, Blindern, NO-1000 Oslo 3, Norway
[33] Dpto. Fisica, Univ. Oviedo, Avda. Calvo Sotelo s/n, ES-33007 Oviedo, Spain
[34] Department of Physics, University of Oxford, Keble Road, Oxford OX1 3RH, UK
[35] Dipartimento di Fisica, Università di Padova and INFN, Via Marzolo 8, IT-35131 Padua, Italy
[36] Rutherford Appleton Laboratory, Chilton, Didcot OX11 OQX, UK
[37] Dipartimento di Fisica, Università di Roma II and INFN, Tor Vergata, IT-00173 Rome, Italy
[38] Dipartimento di Fisica, Università di Roma III and INFN, Via della Vasca Navale 84, IT-00146 Rome, Italy
[39] DAPNIA/Service de Physique des Particules, CEA-Saclay, FR-91191 Gif-sur-Yvette Cedex, France
[40] Instituto de Fisica de Cantabria (CSIC-UC), Avda. los Castros s/n, ES-39006 Santander, Spain
[41] Dipartimento di Fisica, Università degli Studi di Roma La Sapienza, Piazzale Aldo Moro 2, IT-00185 Rome, Italy
[42] Inst. for High Energy Physics, Serpukov P.O. Box 35, Protvino, (Moscow Region), Russian Federation
[43] J. Stefan Institute, Jamova 39, SI-1000 Ljubljana, Slovenia and Department of Astroparticle Physics, School of Environmental Sciences, Kostanjeviska 16a, Nova Gorica, SI-5000 Slovenia,
and Department of Physics, University of Ljubljana, SI-1000 Ljubljana, Slovenia
[44] Fysikum, Stockholm University, Box 6730, SE-113 85 Stockholm, Sweden
[45] Dipartimento di Fisica Sperimentale, Università di Torino and INFN, Via P. Giuria 1, IT-10125 Turin, Italy
[46] Dipartimento di Fisica, Università di Trieste and INFN, Via A. Valerio 2, IT-34127 Trieste, Italy
and Istituto di Fisica, Università di Udine, IT-33100 Udine, Italy
[47] Univ. Federal do Rio de Janeiro, C.P. 68528 Cidade Univ., Ilha do Fundão BR-21945-970 Rio de Janeiro, Brazil
[48] Department of Radiation Sciences, University of Uppsala, P.O. Box 535, SE-751 21 Uppsala, Sweden
[49] IFIC, Valencia-CSIC, and D.F.A.M.N., U. de Valencia, Avda. Dr. Moliner 50, ES-46100 Burjassot (Valencia), Spain
[50] Institut für Hochenergiephysik, Österr. Akad. d. Wissensch., Nikolsdorfergasse 18, AT-1050 Vienna, Austria
[51] Inst. Nuclear Studies and University of Warsaw, Ul. Hoza 69, PL-00681 Warsaw, Poland
[52] Fachbereich Physik, University of Wuppertal, Postfach 100 127, DE-42097 Wuppertal, Germany
[53] On leave of absence from IHEP Serpukhov
[54] Now at University of Florida

1 Introduction

In models including supersymmetry (SUSY), it is often assumed that the messengers of supersymmetry breaking couple to the observable sector with interactions of gravitational strength and that the SUSY breaking scale in the hidden sector is of the order of 10^{11} GeV. An alternative possibility is that supersymmetry is broken at some lower scale (below 10^7 GeV), and that the ordinary gauge interaction acts as the messenger of supersymmetry breaking [1,2]. In this case, the gravitino, $\tilde{G}$, is naturally the lightest supersymmetric particle (LSP) and the lightest Standard Model superpartner is the next to lightest supersymmetric particle (NLSP). Thus, the NLSP is unstable and decays to its Standard Model (SM) partner and a gravitino.

Since the gravitino couplings are in general, with the exception of the so-called ultra-light gravitino scenarios, suppressed compared to electroweak and strong interactions, decays to the gravitino are in general only relevant for the NLSP and therefore the production and decay of supersymmetric particles at high energy colliders would generally take place through Standard Model couplings [1]. The supersymmetric particles decay into the NLSP, which eventually decays to its SM partner and a gravitino. The specific signatures of such decays depend crucially on the quantum numbers and composition of the NLSP.

Although most of the attention has been focused on the case where the neutralino is the NLSP, it is also possible that the NLSP is any other sparticle, and in particular a charged slepton. The number of generations of supersymmetry breaking messengers in minimal models, n, determines over most of the parameter space which particle is the NLSP [3–6]. For example, for one generation of messengers, the lightest neutralino tends to be the NLSP, while for two or more generations, right handed sleptons are favoured. Moreover, when left-right sfermion mixing [7] occurs, the corresponding $\tilde{\tau}$ state, $\tilde{\tau}_1$, becomes the NLSP.

Throughout this work, it is assumed that the $\tilde{\tau}_1$ is the NLSP and that the lightest neutralino, $\tilde{\chi}_1^0$, is the *next-to*-NLSP (NNLSP). The $\tilde{\tau}_1$ width is given (independently of the $\tilde{\tau}$ mixing) by the two-body equation:

$$\Gamma(\tilde{\tau}_1 \to \tau + \tilde{G}) = \frac{m_{\tilde{\tau}_1}^5}{48\pi M_p^2 m_{\tilde{G}}^2} \tag{1}$$

where $m_{\tilde{\tau}_1}$ is the mass of the $\tilde{\tau}_1$, $m_{\tilde{G}}$ is the mass of the $\tilde{G}$ and M_p is the Planck mass (2.4×10^{18} GeV). In the last equation, the mass of the τ has been neglected. The mean decay length obtained from equation (1):

$$L = 1.76 \times 10^{-3} (E^2/m_{\tilde{\tau}_1}^2 - 1)^{\frac{1}{2}} \left(\frac{m_{\tilde{\tau}_1}}{100\,\mathrm{GeV/c^2}}\right)^{-5} \left(\frac{m_{\tilde{G}}}{1\,\mathrm{eV/c^2}}\right)^{2} \ \mathrm{cm}, \tag{2}$$

depends strongly on $m_{\tilde{\tau}}$, $m_{\tilde{G}}$ and the energy of the $\tilde{\tau}_1$, E. The dependence of the mean decay length, L, on $m_{\tilde{G}}$ could be also interpreted in terms of the supersymmetry breaking scale, $\sqrt{F}$, through the relation:

$$m_{\tilde{G}} = \frac{F}{\sqrt{3} M_p} \simeq 2.5 \left(\frac{\sqrt{F}}{100\,\mathrm{TeV}}\right)^{2} \ \mathrm{eV/c^2} \tag{3}$$

For $\sqrt{F} \lesssim 1000$ TeV ($m_{\tilde{G}} \lesssim 250$ eV), the decay can take place within the detector. This range of $\sqrt{F}$ is in fact consistent with astrophysical and cosmological considerations [8].

[1] One exception to this rule being the process $e^+e^- \to Z^*/\gamma^* \to \tilde{G}\tilde{\chi}_1^0$ for the case of ultra-light $\tilde{G}$ scenarios.

Two searches are presented here. Firstly, $\tilde{\chi}_1^0$ pair production with $\tilde{\chi}_1^0$ decaying to $\tilde{\tau}_1\tau$ and $\tilde{\tau}_1$ then decaying promptly into $\tau\tilde{G}$. The signature of the signal would be four τ's with missing energy and momentum from the two gravitinos (in addition to the energy and momentum carried away by the neutrinos of the decay of the τ's).

The second search concerns $\tilde{\tau}_1$ pair production followed by the decays $\tilde{\tau}_1 \to \tau\tilde{G}$ within the detector volume. The signature of such an event will be a track of a charged particle with a kink or a decay vertex when the $\tilde{\tau}_1$ decays inside the tracking devices. If the decay length is too short (small $m_{\tilde{G}}$) to allow for the reconstruction of the $\tilde{\tau}_1$ track, only the decay products of the τ will be seen in the detector, and the search will then be based on track impact parameter. However, if the decay takes place outside the tracking devices (large $m_{\tilde{G}}$), the signature will be that of a heavy charged particle already studied in DELPHI [9]. For very light $m_{\tilde{G}}$ the limits from the search for MSSM stau can be applied [10]. All these searches have been combined to obtain a limit on $m_{\tilde{\tau}_R}$ independent of the $\tilde{G}$ mass.

The data samples and event selections are respectively described in sections 2 and 3, while the results are presented in section 4. It will be seen in section 4 that these two searches, together with those for $\tilde{\chi}_1^0 \to \gamma\tilde{G}$ [11] (in the $\tilde{\chi}_1^0$ NLSP scenario) and promptly decaying $\tilde{\tau}_1$ pair production [10] complement each other for different domains of the gravitino mass.

2 Event sample and experimental procedure

The search for neutralino pair production is based on data collected by the DELPHI experiment during 1996 and 1997 at centre-of-mass energies of 161, 172 and 183 GeV. The total integrated luminosities for the three centre-of-mass energies are 9.7, 10.4 and 53.9 pb^{-1} respectively. The search for stau pair production with big impact parameters and secondary vertices is based on data collected by the DELPHI experiment during 1997 since the results obtained with the data collected in 1995 (at $\sqrt{s} = 130 - 136$ GeV) and 1996 are already published in [12]. The present analysis updates those results. The search for stau pair production with small impact parameters is based on data collected from 1995 to 1997. A detailed description of the DELPHI detector can be found in [13] and its performance in [14].

To evaluate the signal efficiencies and background contaminations, events were generated using different programs, all relying on `JETSET` 7.4 [15], tuned to LEP 1 data [16] for quark fragmentation. The program `SUSYGEN` [17] was used to generate the neutralino pair events and their subsequent decay products. In order to compute detection efficiencies, a total of 3000, 10000 and 14000 events were generated with centre-of-mass energies of 161, 172 and 183 GeV respectively, and masses 47 GeV/$c^2 \leq m_{\tilde{\tau}_1} + 2$ GeV/$c^2 \leq m_{\tilde{\chi}_1^0} \leq \sqrt{s}/2$. A stau pair sample of 18000 events (subdivided in 15 samples) was produced with `PYTHIA 5.7` [15] at 183 GeV centre-of-mass energy, the staus having mean decay lengths from 0.25 to 1000 cm and masses from 40 to 90 GeV/c^2. Another sample of 35000 stau pairs was produced with `SUSYGEN` for the small impact parameter search (see below), with centre-of-mass energies ranging from 130 GeV up to 183 GeV.

The background process $e^+e^- \to q\bar{q}(n\gamma)$ was generated with `PYTHIA 5.7`, while `DYMU3` [18] and `KORALZ` [19] were used for $\mu^+\mu^-(\gamma)$ and $\tau^+\tau^-(\gamma)$, respectively. The generator of reference [20] was used for $e^+e^- \to e^+e^-$ events.

Processes leading to four-fermion final states, $(Z/\gamma)^*(Z/\gamma)^*$, where * means of-the-mass-shell, W^+W^-, $We\nu_e$ and Ze^+e^-, were also generated using `PYTHIA`. The calculation

of the four-fermion background was verified using the program EXCALIBUR [21], which consistently takes into account all amplitudes leading to a given four-fermion final state.

Two-photon interactions leading to hadronic final states were generated using TWOGAM [22], separating the VDM, QPM and QCD components. The generators of Berends, Daverveldt and Kleiss [23] were used for the leptonic final states.

The cosmic radiation background was studied using the data collected before the beginning of the 1997 LEP run.

The generated signal and background events were passed through the detailed simulation [14] of the DELPHI detector and then processed with the same reconstruction and analysis programs used for real data.

3 Data selection

3.1 Neutralino pair production

In this section, the selections used to search for the process $e^+e^- \to \tilde{\chi}_1^0\tilde{\chi}_1^0 \to \tilde{\tau}_1\tau\tilde{\tau}_1\tau \to \tau\tilde{G}\tau\tau\tilde{G}\tau$ are presented.

The reconstructed tracks of charged particles were required to have momenta above 100 MeV/c and impact parameters below 4 cm in the transverse plane and below 10 cm in the longitudinal direction. The relative error on the measurement of the momentum was to be smaller than 100%. Clusters in the calorimeters were interpreted as neutral particles if they were not associated to charged particles and if their energy exceeded 100 MeV. All charged and neutral particles that satisfy these criteria are considered good particles and they are used to compute the relevant event quantities. To assure good quality of the data, the ratio of good to total number of tracks was required to be above 0.7. Tracks that did not pass quality selection but had an associated calorimetric energy of at least 2 GeV had their angles taken from those of the track, but their momentum was recomputed as that of the calorimetric measurement. Such tracks were not included in the good sample. Events had to have between four and ten good charged particle tracks. In addition, it was required that the thrust be less than 0.99. The transverse momentum, computed as the transverse component with respect to the beam axis of the vector sum of the momenta of good charged and neutral particles, p_T, had to be bigger than 3 GeV/c. And the absolute value of the cosine of the polar angle of the missing momentum vector be less than 0.95. Very forward-going events were eliminated by requiring that the energy in a cone of 30°, E_{30}, around the beam-pipe to be less than 70% of the total visible energy, E_{vis}. With this preselection, the total number of simulated background events and real data events was reduced by a factor of about 6000. Only events passing these pre-selections were analysed further.

The selection takes advantage of the fact that signal events can be separated into two different kinematic regions of the ($m_{\tilde{\chi}_1^0}$,$m_{\tilde{\tau}_1}$) space: when the mass difference $\Delta m = m_{\tilde{\chi}_1^0} - m_{\tilde{\tau}_1}$ is bigger than about 10 GeV/c^2, all four τ's carry similar momenta. When the difference becomes smaller, the two τ's coming from the decay of the $\tilde{\tau}_1$ tend to be the most energetic, increasingly so as the $\tilde{\chi}_1^0$ mass increases. The Durham algorithm [25] was used to divide the event in four jets by allowing y_{cut} to vary as a free variable. Numbering the jets from 1 to 4 with $\mathrm{E}_1 > \mathrm{E}_2 > \mathrm{E}_3 > \mathrm{E}_4$, a variable r was defined as:

$$r = \frac{\mathrm{E}_3 + \mathrm{E}_4}{\mathrm{E}_1 + \mathrm{E}_2} \ . \tag{4}$$

An example of the distribution of r for simulated samples with two values of Δm can be seen in figure 1. It should be noticed that the distribution of r shifts towards lower values with increasing neutralino masses. The simulated background samples were then divided into two samples above and below $r = 0.1$ and different requirements were imposed in the two cases.

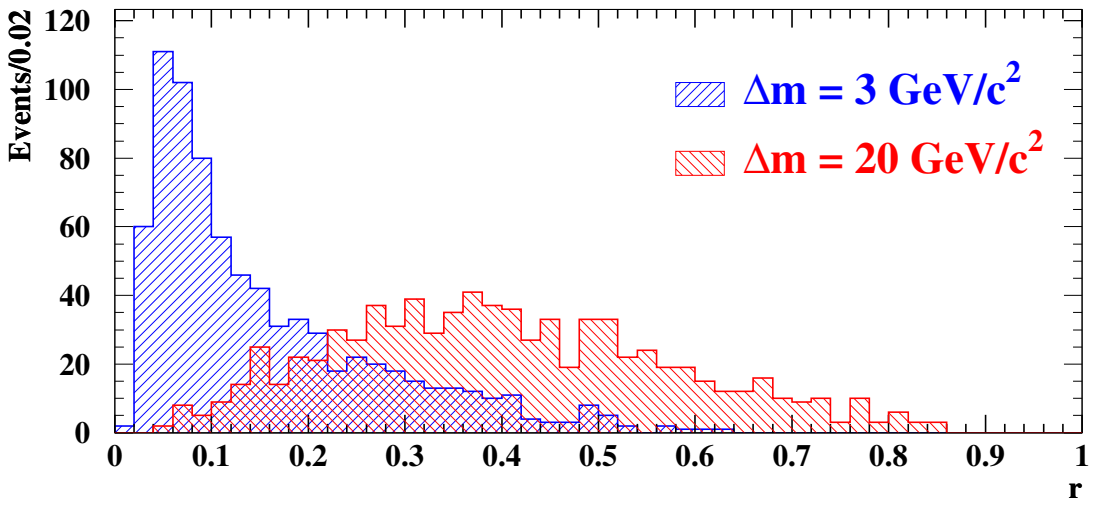

Figure 1: Two examples of the distribution of the variable r (see text). The positive-slope hatched histogram shows r for $\Delta m = 3$ GeV/c^2. The negative-slope hatched histogram shows r for $\Delta m = 20$ GeV/c^2.

Two sets of cuts were applied in order to reduce the $\gamma\gamma$ and $f\bar{f}(\gamma)$ backgrounds and a third set of cuts to select events according to their topology:

1- Cuts against $\gamma\gamma$ backgrounds: the transverse energy, E_T, should be bigger than 11 GeV for $r > 0.1$ ($E_T > 12$ GeV for $r \leq 0.1$). The energy in a cone of 30° around the beam axis was further restricted to be less than 60% of the total visible energy to avoid possible bias from the Monte Carlo samples. The missing mass should be smaller than $0.88\sqrt{s}$ ($0.9\sqrt{s}$). The momentum of the charged particle with largest momentum should be bigger than 4 GeV/c (3 GeV/c). These cuts reduced the $\gamma\gamma$ background by a factor of the order of 30.

2- Cuts against $f\bar{f}(\gamma)$ backgrounds: the number of good tracks should be smaller than 7 (9). The maximum thrust was further reduced from 0.99 to 0.975. Dividing each event into two jets with the Durham algorithm, its acoplanarity should be bigger than 8°. The missing mass of the events should be bigger than $0.3\sqrt{s}$. After these cuts, the $f\bar{f}(\gamma)$ background was reduced by a factor of the order of 15.

3- Cuts based on topology: signal events tend naturally to cluster into a 4-jet topology. All jets should be at least 17° away from the beam direction. When reduced by the jet algorithm into a 2-jet configuration, the charged particles belonging to each of these jets should be in a cone broader than 20°. Finally, the axes of each of the four jets should be separated from the others at least by 8° (4°).

Figures 2 to 4 show some of the distributions relevant for these selection criteria at $\sqrt{s} = 183$ GeV. Table 1 shows the effect of these cuts at $\sqrt{s} = 183$ GeV on the data, expected background and the signal for $m_{\tilde{\chi}_1^0} = 75$ GeV/c^2 and $m_{\tilde{\tau}_1} = 55$ GeV/c^2. The discrepancy between data and simulation on the last bin of figure 2-a is attributed to the poor description of $\gamma\gamma$ events in the simulation.

Cut	$\gamma\gamma$	$ff\gamma$	4-fermion	Total MC	Data	Signal
pre-selection	496 ± 16	44.5 ± 1.5	13.1 ± 0.6	554 ± 16	567	61.4%
1	18 ± 2	40.6 ± 1.4	12.1 ± 0.6	70.8 ± 2.6	84	59.2%
2	2.2 ± 0.6	2.9 ± 0.4	4.5 ± 0.4	9.6 ± 0.8	12	45.4%
3	0	0.23 ± 0.09	0.27 ± 0.07	0.50 ± 0.11	2	38.3%

Table 1: Number of events remaining in the data and simulated samples at $\sqrt{s} = 183$ GeV after various stages of the selection procedure described in the text. The signal efficiencies corresponds to $m_{\tilde{\chi}_1^0} = 75$ GeV/c^2 and $m_{\tilde{\tau}_1} = 55$ GeV/c^2.

After these cuts, an efficiency between 25 and 45% was obtained for the signal events, and estimated backgrounds of 0.12 ± 0.08, 0.15 ± 0.09 and 0.50 ± 0.11 events at $\sqrt{s} =$ 161, 172 and 183 GeV, respectively.

3.2 Stau pair production

This section describes the selection criteria used in the search for the process $e^+e^- \to \tilde{\tau}_1\tilde{\tau}_1 \to \tau\tilde{G}\tau\tilde{G}$. As described in section 1, the mean life-time of the $\tilde{\tau}_1$ depends on the mass of the gravitino. Thus, for a gravitino with a mass of the order of a few hundred eV/c^2 or more, the stau would be sufficiently long lived to decay outside the detector. When the mass of the gravitino is between a few eV/c^2 and a few hundred eV/c^2, one or both staus would decay in flight in some part of the detector, creating a well defined secondary vertex. The search for these decays is described in subsection 3.2.1. If the mass of the gravitino is even smaller, stau pair production would produce displaced vertices. This search is described in subsections 3.2.2 and 3.2.3.

3.2.1 Search for secondary vertices

This analysis exploits a peculiarity of the $\tilde{\tau}_1 \to \tau\tilde{G}$ topology in the case of intermediate mass gravitinos, namely, one or two tracks coming from the interaction point and at least one of them with either a secondary vertex or a kink.

Rather loose preselection cuts, similar to those presented in reference [12] were imposed on the events in order to suppress the low energy background (beam-gas, beam-wall, etc), $\gamma\gamma$, e^+e^- and hadronic events. To compute the following quantities the reconstructed tracks of charged particles were required to have momenta above 100 MeV/c and impact parameters below 4 cm in the transverse plane and below 10 cm in the longitudinal direction. Clusters in the calorimeters were interpreted as neutral particles if they were not associated to charged particles and if their energy exceeded 100 MeV. However, no quality requirements were imposed on the reconstructed tracks in the following stages.

- Charged particle multiplicity between 1 and 10;
- visible energy above 10 GeV;

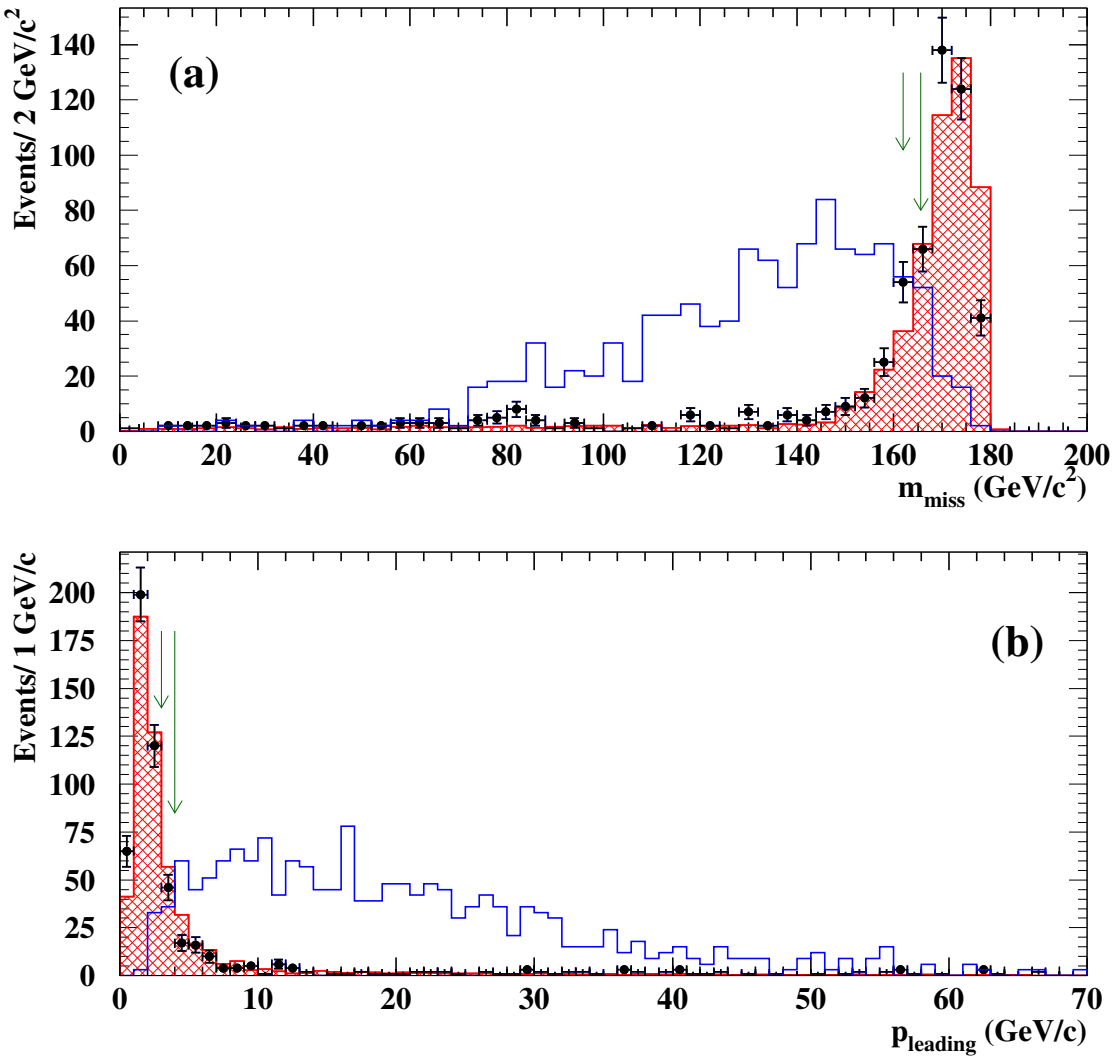

Figure 2: (a) missing mass and (b) momentum of the leading charged particle, for data (dots), Standard Model simulation (cross-hatched histogram) and one of the simulated signals with cross-section not to scale (blank histogram) after preselection at $\sqrt{s} = 183$ GeV. The arrows indicate selection criteria imposed as explained in the text.

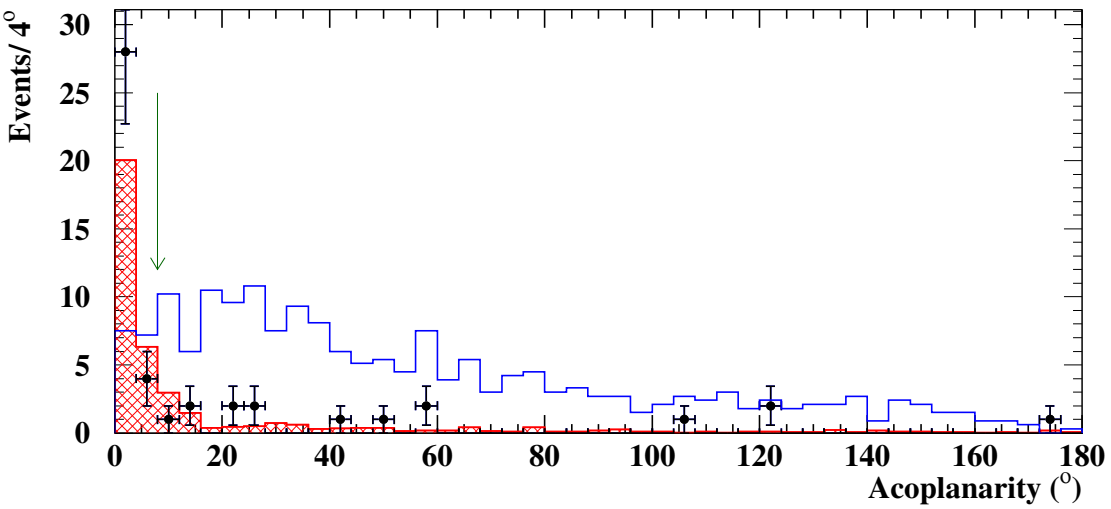

Figure 3: Acoplanarity of data (dots), Standard Model background simulation (cross-hatched histogram) and one of the simulated signals with cross-section not to scale (blank histogram) at $\sqrt{s} = 183$ GeV, after the cut to remove $\gamma\gamma$ events. The arrow indicates selection criterion imposed as explained in the text.

- total electromagnetic energy below 40 GeV;
- transverse momentum, computed as the transverse component with respect to the beam axis of the vector sum of the momenta of charged and neutral particles, p_T, greater than 5 GeV/c;
- energy measured in the very forward calorimeters below 10 GeV.

These preselection cuts leave about 0.6% of the whole data sample.

The tracks of the events that survived the preselection cuts were grouped in clusters according to their first measured point (starting point). This clustering procedure is described in [26]. Each cluster contained all tracks whose starting points differ by less than 2 cm. The starting point of a cluster was defined as the average of the starting points of its tracks. This procedure allowed for clusters with a single track if its momentum was larger than 1.5 GeV/c. Events were rejected if more than 6 tracks were not grouped in clusters or no cluster was found. A cluster with only one track was considered a $\tilde{\tau}_1$ candidate track if its trajectory was compatible with that of a particle coming from the interaction point (according to the selection criteria described in reference [12]) and its momentum was greater than 2 GeV/c.

For each such $\tilde{\tau}_1$ candidate, a search was made for a second cluster with starting point radius in the transverse plane (xy plane) greater than that of the first measured point of the track of the $\tilde{\tau}_1$ candidate, and an angular separation between the directions defined by the beam spot and the cluster starting points smaller than 90° in the xy plane. This second cluster was assumed to be formed by the decay products of the τ coming from the $\tilde{\tau}_1 \to \tau\tilde{G}$ process. Therefore, the $\tilde{\tau}_1$ candidate and the τ cluster had to define a secondary vertex. If the τ cluster included more than one charged particle, only the one with the highest momentum was used to search for the decay vertex or kink (crossing point with the $\tilde{\tau}_1$ track).

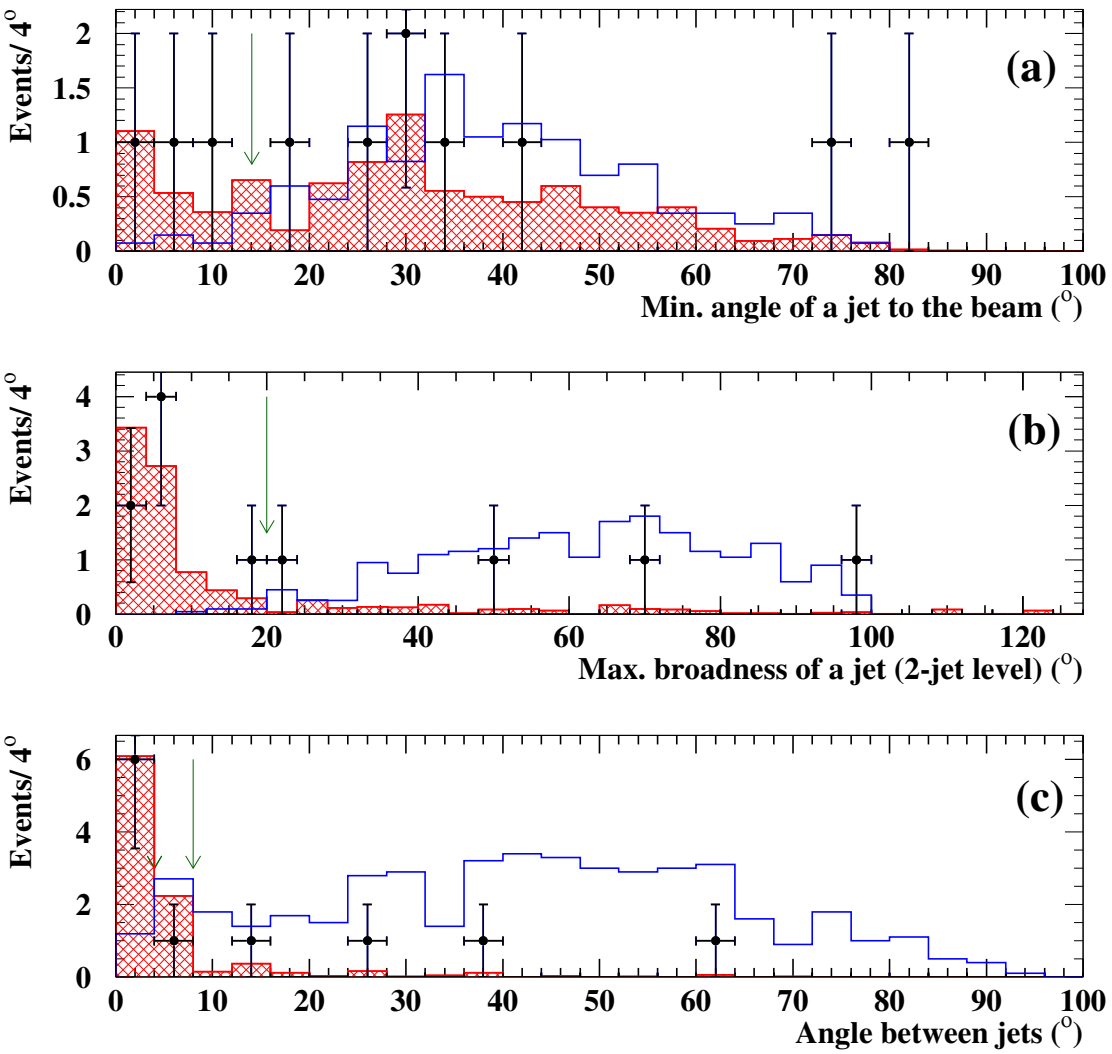

Figure 4: (a) minimum angle of a jet to the beam, (b) maximum angular broadness of a jet at the 2-jet level and (c) angle between jets, for data (dots), Standard Model background simulation (cross-hatched histogram) and one of the simulated signals with cross-section not to scale (blank histogram) at $\sqrt{s} = 183$ GeV, after the cut to remove $f\bar{f}(\gamma)$ events. The arrows indicate selection criteria imposed as explained in the text.

The tracks were parametrised with respect to their perigee [27] to calculate the point of closest approach between the two tracks (the candidate $\tilde{\tau}_1$ track and the selected track from the candidate τ cluster). The conditions to define a good crossing point between the track of the $\tilde{\tau}_1$ and the selected track of the τ decay candidates are described in reference [12].

Fake decay vertices could be present amongst the reconstructed secondary vertices, being produced by particles interacting in the detector material or by radiated photons if the particle trajectory was reconstructed into two separated tracks. To eliminate these classes of events, additional requirements were imposed:

- to reject hadronic interactions, any reconstructed hadronic interaction (secondary vertices reconstructed in region where there is material) must be outside a cone of half angle 5° around the kink direction;
- to reject photon radiation in the case of τ clusters with only one track, there had to be no neutral particle in a 3° cone around the direction defined by the difference between the $\tilde{\tau}_1$ momentum and the momentum of the τ daughter calculated at the crossing point;
- to reject segmented tracks, the angle between the tracks used to define a vertex had to be larger than 6°.

If no pair of tracks was found to survive these conditions, the event was rejected. Figure 5 shows the distribution of these three angles for real data, expected Standard Model background simulation and simulated signal for $m_{\tilde{\tau}_1} = 60$ GeV/c^2 decaying with a mean distance of 50 cm. The excess of data in the first bins of figure 5 (c) is due to underestimation in the simulation of mismatchings between the tracking devices.

One event in real data was found to satisfy all the conditions described above. The event was the superposition of a low energy event with a cosmic muon crossing the detector. However, the two tracks of the cosmic muon follow the cosmic muon rejection criteria used on subsection 3.2.2 based on impact parameter and on acollinearity. Thus, the event will not be considered as a candidate. This kind of events was not simulated and therefore its removal does not affect the calculated efficiencies.

The vertex reconstruction was sensitive to decay lengths in the xy plane, R, between 15 cm and 90 cm. Within this region a vertex was reconstructed with an efficiency of ~54% since the VD (Vertex Detector) and the ID (Inner Detector) were needed to reconstruct the $\tilde{\tau}_1$ track and the TPC (Time Projection Chamber) to reconstruct the decay products. The efficiency is flat inside the sensitive region and drops to zero for $\tilde{\tau}_1$'s decaying near the outer surface of the TPC. The shape of the efficiency distribution was independent of the $\tilde{\tau}_1$ mass; it simply scaled down near the kinematic limit. The loss of efficiency near the kinematic limit is due to the fact that the $\tilde{\tau}_1$ boost is smaller and the vertex reconstruction less efficient when the angles between the $\tilde{\tau}_1$ and the τ products increase.

The efficiencies for different mean decay lengths and $\tilde{\tau}_1$ masses were calculated by applying the above selections to the simulated signal samples. For a 60 GeV/c^2 $\tilde{\tau}_1$ with mean decay length of 50 cm the vertex search efficiency is of the order of 55%.

3.2.2 Large impact parameter search

To investigate the region of low gravitino masses (short decay lengths) the previous search was extended to the case of the $\tilde{\tau}_1$ decaying between 0.25 cm and around 10 cm. In this case the $\tilde{\tau}_1$ track was not reconstructed in the ID and only the τ decay products

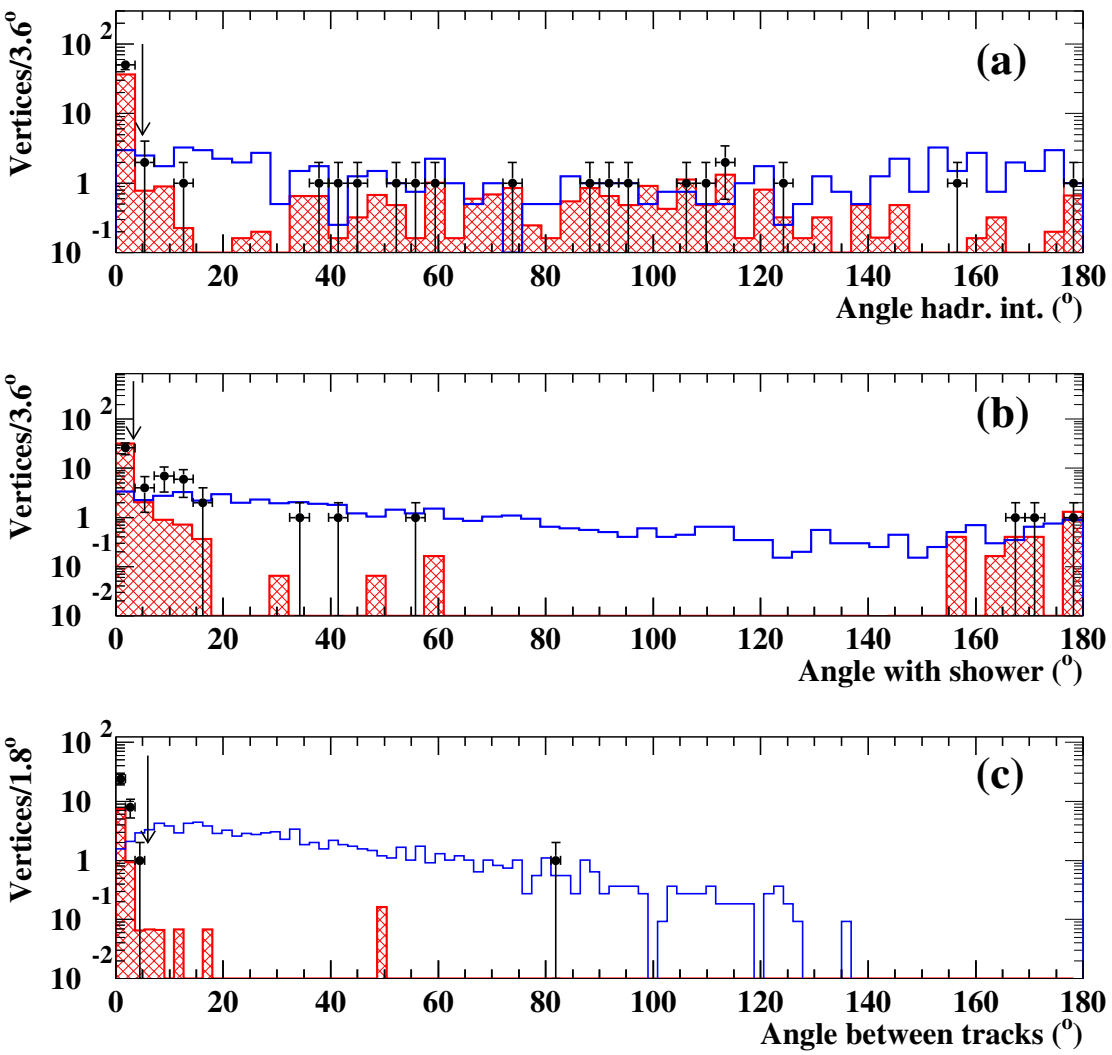

Figure 5: (a) angle between the hadronic interaction and the reconstructed vertex, (b) angle between the electromagnetic shower and the direction defined by the difference between the momenta of $\tilde{\tau}_1$ and its associated τ, defined at the crossing point, and (c) angle between the tracks of the kink, for real data (dots), expected Standard Model background (cross-hatched histogram) and simulated signal for $m_{\tilde{\tau}_1} = 60$ GeV/c^2 decaying with a mean distance of 50 cm (blank histogram). The arrows indicate selection criteria imposed as explained in the text.

were detected. The events used in this search contained exactly two single track clusters (i.e. two charged particles with momentum larger than 1.5 GeV/c and a distance between starting points greater than 2 cm) which were acollinear and had large impact parameters[2]. Cosmic rays, badly reconstructed tracks or interactions in the detector material could result in large impact parameters. However, the two tracks in a cosmic event usually have impact parameters of the same order and opposite sign. The acollinearity in back-to-back events with badly reconstructed tracks or interactions was always small. Figure 6 shows the scatter plot of the maximum impact parameter versus the minimum one in the $R\phi$ plane. Figure 7 shows the acollinearity distribution for events with two tracks in the TPC. Simulated signal events with $m_{\tilde{\tau}_1} = 60$ GeV/c^2 and a mean decay length of 2.5 cm are compared with cosmic muon events, simulated Standard Model background and real data. The data points in figure 7 contain cosmic radiation events that are not simulated.

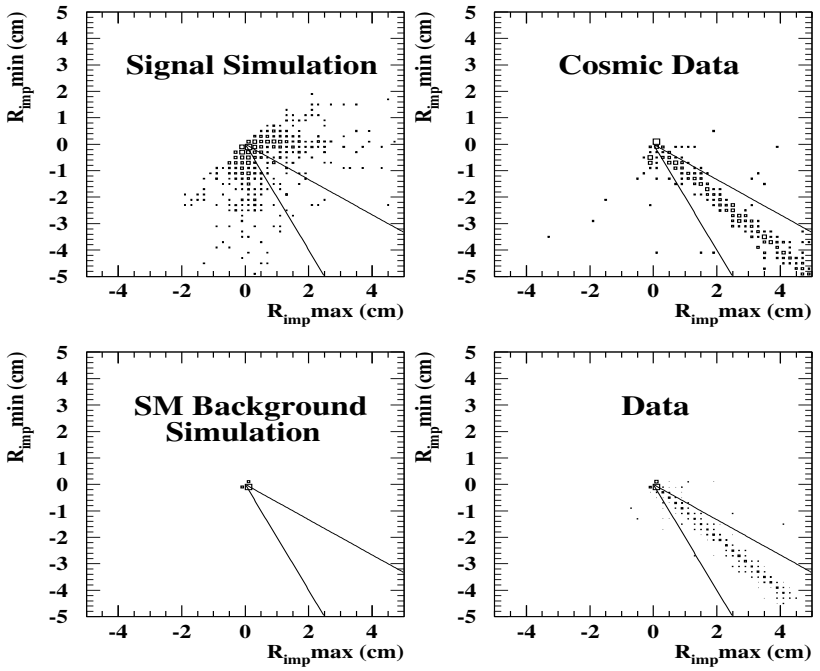

Figure 6: Impact parameters of two track events for a simulated signal of $m_{\tilde{\tau}_1} = 60$ GeV/c^2 with mean decay length of 2.5 cm, cosmic muons, Standard Model expected background and real data. It is plotted the maximum impact parameter versus the minimum one in the $R\phi$ plane. The area between the lines was excluded by the cosmic rejection criteria as described in the text.

The impact parameter search was only applied to those events accepted by the same general requirements as in the search for secondary vertices, and not selected by the vertex analysis. The events were accepted as candidates if:

- the first measured point of at least one of the tracks was within 12 cm of the beam spot in the plane transverse to the beam axis;

[2] The impact parameter is defined as the distance of closest approach of a charged particle to the reconstructed primary vertex. The impact parameters in the $R\phi$ and Rz plane are evaluated separately. The sign of the impact parameter is defined with respect to the jet direction. It is positive if the vector joining the primary vertex to the point of closest approach of the track is less than 90° from the direction of the jet to which the track belongs. In events with two particles, each reconstructed track is considered as a jet.

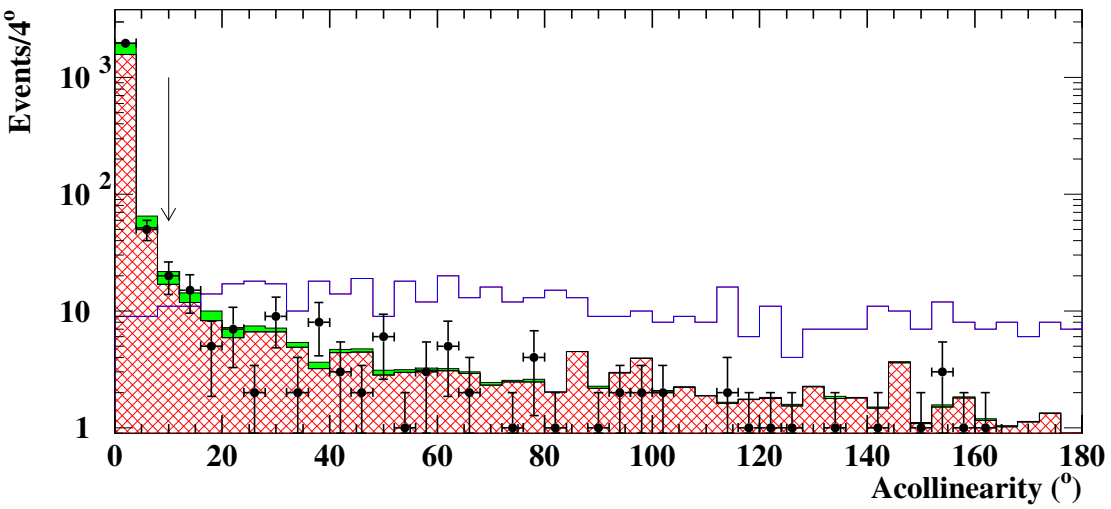

Figure 7: Acollinearity for real data (dots), a simulated signal of $m_{\tilde{\tau}_1} = 60$ GeV/c^2 decaying with a mean distance of 50 cm (blank histogram), and expected simulated Standard Model background (cross-hatched histogram) plus cosmic background (dark grey histogram). This last background is normalized in order to make the first bin of SM background plus cosmic radiation coincide with the corresponding value of real data. The selection on this variable is explained in the text and is shown with an arrow.

- both tracks were reconstructed in the TPC to guarantee a good track reconstruction quality;
- at least one of the tracks had an impact parameter larger than 0.2 cm in the plane transverse to the beam axis, to remove standard model events;
- the ratio of the maximum impact parameter over the minimum impact parameter in the $R\phi$ plane was smaller than -1.5 or larger than -0.5, to reject cosmic rays;
- the acollinearity between the two tracks was larger than 10°;
- the angle defined by the directions of the starting points of the tracks with respect to the the beam-spot was larger than 3°.

The efficiencies were derived for the different $\tilde{\tau}_1$ masses and decay lengths by applying the same selection to the simulated signal events. The maximum efficiency was 29.2%, corresponding to a mean decay length of 2.5 cm, decreasing very fast for lower decay lengths due to the cut on minimum impact parameter. For longer decay lengths, the appearance of reconstructed $\tilde{\tau}_1$ tracks in combination with the cut on the maximum amount of charged tracks caused the efficiency to decrease smoothly. This decrease is compensated by a rising efficiency in the search for vertices. No dependence on the $\tilde{\tau}_1$ mass was found far from the kinematic limit. The losses of efficiency for $\tilde{\tau}$ masses near the kinematic limit and due to initial state radiation were also considered.

Trigger efficiencies were studied, simulating the DELPHI trigger response to the events selected by the vertex search and by the large impact parameter analysis, and were found to be around 99%.

No events in the real data sample were selected with the above criteria. The number of expected background events at $\sqrt{s} = 183$ GeV is shown in Table 2 for the combination of the vertex and large impact parameter searches.

Observed events	0
Total background	$0.63^{+0.55}_{-0.12}$
$Z^*/\gamma \to (\tau\tau)(n\gamma)$	$0.07^{+0.16}_{-0.06}$
$Z^*/\gamma \to (ee)(n\gamma)$	$0.09^{+0.19}_{-0.03}$
4-fermion (except $\gamma\gamma$)	$0.10^{+0.12}_{-0.06}$
$\gamma\gamma \to \tau^+\tau^-$	$0.20^{+0.27}_{-0.06}$
$\gamma\gamma \to e^+e^-$	$0.17^{+0.39}_{-0.05}$

Table 2: The number of observed events at $\sqrt{s} = 183$ GeV, together with the total number of expected background events and the expected numbers from the individual background sources, for both large impact parameter and secondary vertex searches combined.

3.2.3 Small impact parameter search

The large impact parameter search can be extended further down to mean decay lengths of around 0.1 cm. Charged particles were selected if their impact parameter was less than 10 cm in the transverse plane and less than 15 cm in the longitudinal direction and their polar angle between 20° and 160°. Their measured momentum was required to be larger than 400 MeV/c with relative error less than 100% and track length larger than 30 cm. Any calorimetric deposit associated to a discarded charged particle was assumed to come from a neutral particle.

This search was restricted to events with 2 to 4 charged particles and missing energy larger than 0.3 $\sqrt{s}$. The $\gamma\gamma$ events were suppressed by requiring that the visible energy (E_{vis}) be bigger than 0.08 $\sqrt{s}$ and the transverse missing momentum larger than 0.03 $\sqrt{s}$. The polar angle of the missing momentum was required to be between 30° and 150° and the total energy in the forward and backward regions (E_{30}) was required to be less than 10% of the total visible energy in the event.

The events were then divided into two hemispheres using the thrust axis. The total momentum of charged and neutral particles in each hemisphere was computed and used to define the events' acollinearity. Standard $e^+e^- \to f\bar{f}(\gamma)$ processes and cosmic ray events were reduced by requiring the acollinearity to be greater than 10°. The charged particle with largest momentum in each hemisphere was selected (leading particle). The following quality requirements were only applied to the leading charged particles: the first measured point of the tracks had to be within 50 cm of the beam spot in the xy plane, the tracks were required to have at least a track segment beyond the ID detector, and away from insensitive regions of the electromagnetic calorimeter. In addition, at least one of the tracks was required to be reconstructed with the TPC.

The standard $e^+e^- \to f\bar{f}(\gamma)$ and cosmic backgrounds were reduced by requiring the angle between the leading particles in the xy plane to be less than 3 radians. $q\bar{q}(\gamma)$ and 4-fermion events were further rejected by requiring $\sqrt{p_1^2 + p_2^2}$ (where p_1 and p_2 are the momenta of the leading particles) to be smaller than $0.03\sqrt{s}$. To reduce Bhabha events

the total electromagnetic energy of the leading particles ($E_{em1} + E_{em2}$) had to be smaller than $0.35\sqrt{s}$. By requiring that any leading track with an impact parameter larger than 1 cm in the xy plane should be reconstructed by the TPC and at least another detector, the residual cosmics were rejected. Finally, γ conversion events with only two tracks were rejected by requiring the angle between tracks at their perigee to be greater than 1°.

The background left after the selection described above consists mainly of events containing τ pairs in the final state ($\gamma^*/Z^* \to \tau\tau$ and $WW \to \tau\nu\tau\nu$). To reject these events, the variable $b_c = \sqrt{b_1^2 + b_2^2}$ was used, where b_1 and b_2 are the impact parameters of the leading particles, defined in the xy plane. Figure 8 shows the b_c distribution of the selected real data, the total residual simulated background and the b_c distribution of one set of simulated signal events, with an arbitrary scale. A cut of $b_c \geq 600\mu$m was chosen to reject most of the remaining background.

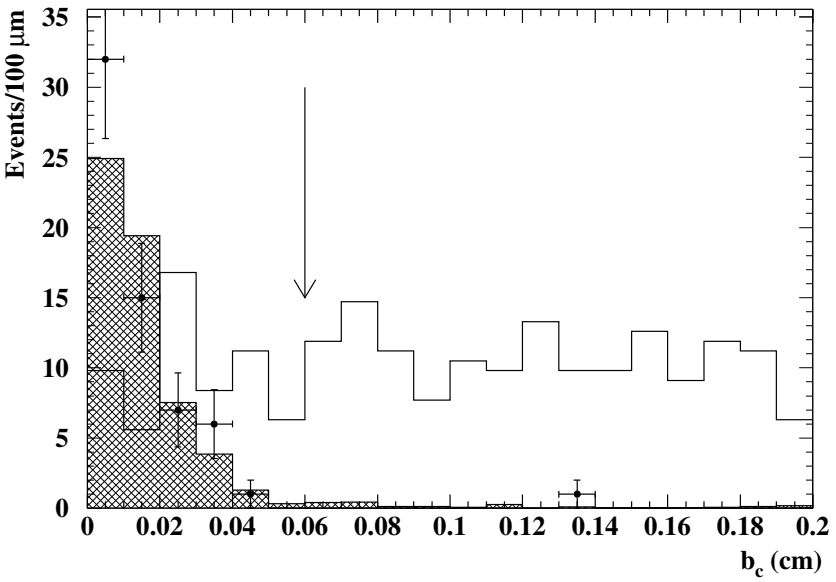

Figure 8: b_c distribution for real data (dots), expected Standard Model background (cross-hatched histogram) and a simulated signal of $m_{\tilde{\tau}_1} = 50$ GeV/c^2 and a mean decay length of $\sim$ 1 cm (in arbitrary scale).

Applying these cuts to the simulated signal events, the efficiency turned out not to depend separately on the centre-of-mass energy and on the $\tilde{\tau}_1$ mass but rather on the $\tilde{\tau}_1$ decay length in the laboratory system, which is determined by both these variables. The maximum efficiency was $\sim$ 40% for a mean decay length of $\sim$ 2 cm. The cut on b_c caused the efficiency to drop at small decay lengths ($\sim$ 15% at 1 mm), whilst at large decay lengths a loss of efficiency was due to the upper impact parameter cut used in the track selection.

The non-negligible background contributions, normalized to the integrated luminosities of the four samples, are shown in table 3 together with the number of selected data events. As expected, the main sources of background come from channels containing τ's in the final state.

	130 GeV + 136 GeV	161 GeV	172 GeV	183 GeV
Observed events	0	0	0	1
Total background	$0.19^{+0.66}_{-0.08}$	$0.33^{+0.19}_{-0.11}$	$0.19^{+0.12}_{-0.05}$	$1.97^{+0.46}_{-0.27}$
$Z^*/\gamma \to (\tau\tau)(n\gamma)$	$0.19^{+0.14}_{-0.08}$	$0.21^{+0.13}_{-0.09}$	$0.07^{+0.07}_{-0.04}$	$0.99^{+0.29}_{-0.22}$
$\gamma\gamma \to \tau^+\tau^-$	$0.00^{+0.65}_{-0.00}$	$0.09^{+0.14}_{-0.06}$	$0.00^{+0.08}_{-0.00}$	$0.20^{+0.33}_{-0.12}$
WW	-	$0.03^{+0.01}_{-0.01}$	$0.12^{+0.04}_{-0.03}$	$0.76^{+0.13}_{-0.11}$
ZZ	-	-	-	$0.02^{+0.02}_{-0.01}$

Table 3: Expected simulated SM background events and selected data events at the various centre-of-mass energies for the small impact parameter search.

4 Results and interpretation

4.1 Neutralino pair production

No event passes the selections at $\sqrt{s} = 161$ or 172 GeV. Two events were observed to pass all the cuts at $\sqrt{s} = 183$ GeV. One of them is shown in fig. 9.

Their main features are listed in Table 4. Both of them can be interpreted as being 4-fermion events. The first event has an electron, a pion, and two unidentified low momentum particles. The event could be described as $\gamma^*\gamma^*$, each virtual photon going into a pair of τs. The second event contains a muon, two energetic electrons and a pion. It could be described as a $Z^*\gamma^*$ event, with $Z^* \to e^+e^-$ and $\gamma^* \to \tau^+\tau^-$.

	Candidate 1	Candidate 2
r	0.14	0.31
p_{T}	8.7 GeV/c	9.2 GeV/c
m_{miss}	139.5 GeV/c^2	63.8 GeV/c^2
Thrust	0.91	0.84
$\mathrm{E}_{30}/\mathrm{E}_{vis}$	0.45	0.62
E_T	28.0 GeV	78.6 GeV
Acoplanarity	8.6°	15.9°
Num. of charged particles	4	6
Min. angle between jets	63°	26.°
P of leading particle	17.8 GeV/c	43.7 GeV/c

Table 4: Some characteristics of the two candidates found at $\sqrt{s} = 183$ GeV.

Since no evidence for a signal was found in the data, a limit on the production cross-section for neutralino pairs was derived for each ($m_{\tilde{\chi}^0_1}$,$m_{\tilde{\tau}_1}$) combination. A statistical error of $\pm 1.5\%$ was assumed for the signal efficiency.

In what follows, the model described in reference [4] will be used in order to derive limits. This is a general model which assumes only radiatively broken electroweak symmetry and null trilinear couplings at the messenger scale. The corresponding parameter space was scanned as follows: $1 \leq n \leq 4$, 5 TeV $\leq \Lambda \leq$ 900 TeV, $1.1 \leq M/\Lambda \leq 9000$, $1.1 \leq \tan\beta \leq 50$, and $\mu > 0$, where n is the number of messenger generations in the model, Λ is the ratio between the vacuum expectation values of the auxiliary component

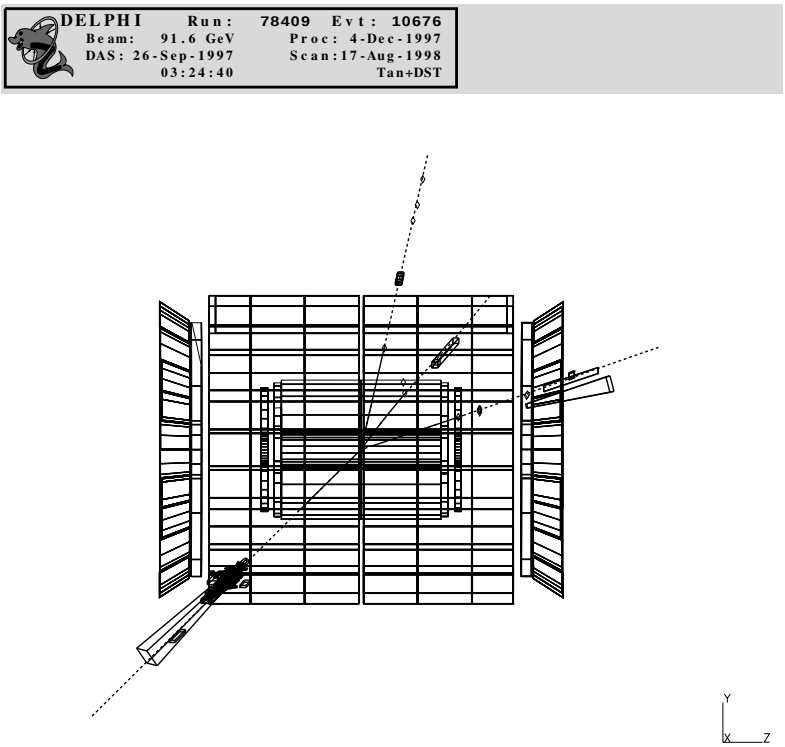

Figure 9: yz view of the second of the two neutralino pair production candidates. From above, clockwise, the particles are identified as a muon, a pion, an electron (with associated radiated photon) and an electron.

superfield and the scalar component of the superfield and M is the messenger mass scale, $\tan\beta$ and μ are defined as for the MSSM.

Figure 10 shows the 95% C.L. upper limit on the $\tilde{\chi}_1^0$ pair production cross-section at $\sqrt{s} = 183$ GeV as a function of $m_{\tilde{\chi}_1^0}$ and $m_{\tilde{\tau}_1}$ after combining the results of the searches at $\sqrt{s} = 161$, 172 and 183 GeV with the maximum likelihood ratio method [28]. For different number of messenger generations, the ratios between production cross sections at different energies are bound to vary within certain limits. The same happens when considering scenarios with higgsino- or gaugino-like neutralinos. Figure 10 presents as an example the case of $n = 3$ and gaugino-like $\tilde{\chi}_1^0$. For the other scenarios considered in this study ($1 \leq n \leq 4$, and gaugino- or higgsino-like neutralinos), the maximum difference with respect to figure 10 occurs in the region where $m_{\tilde{\chi}_1^0} < 80$ GeV/c^2 and $m_{\tilde{\tau}_1} < 65$ GeV/c^2, and is not bigger than 10%.

Given the aforementioned limits on the production cross-section, some sectors of the $(m_{\tilde{\chi}_1^0}, m_{\tilde{\tau}_1})$ space can be excluded. In order to achieve the maximum sensitivity, the results from two other analyses are taken into account. The first is the search for $\tilde{\tau}_1$ pair production in the context of the MSSM. In the case where the MSSM $\tilde{\chi}_1^0$ is massless, the kinematics correspond to the case of $\tilde{\tau}_1$ decaying into a τ and a gravitino, except for spin effects, which are not taken into account in SUSYGEN. The second is the search for lightest neutralino pair production in the region of the mass space where $\tilde{\chi}_1^0$ is the NLSP [11] (the region above the diagonal line, i.e. $m_{\tilde{\tau}} > m_{\tilde{\chi}_1^0}$). Within this zone, the neutralino decays into a gravitino and a photon.

As an illustration, fig. 11 presents the 95% C.L. excluded areas for the case $n = 2$ and gaugino-like neutralinos in the $m_{\tilde{\chi}_1^0}$ *vs.* $m_{\tilde{\tau}_1}$ plane. The positive-slope dashed area is excluded by this analysis. The resulting 95% C.L. lower limit on the mass of the lightest

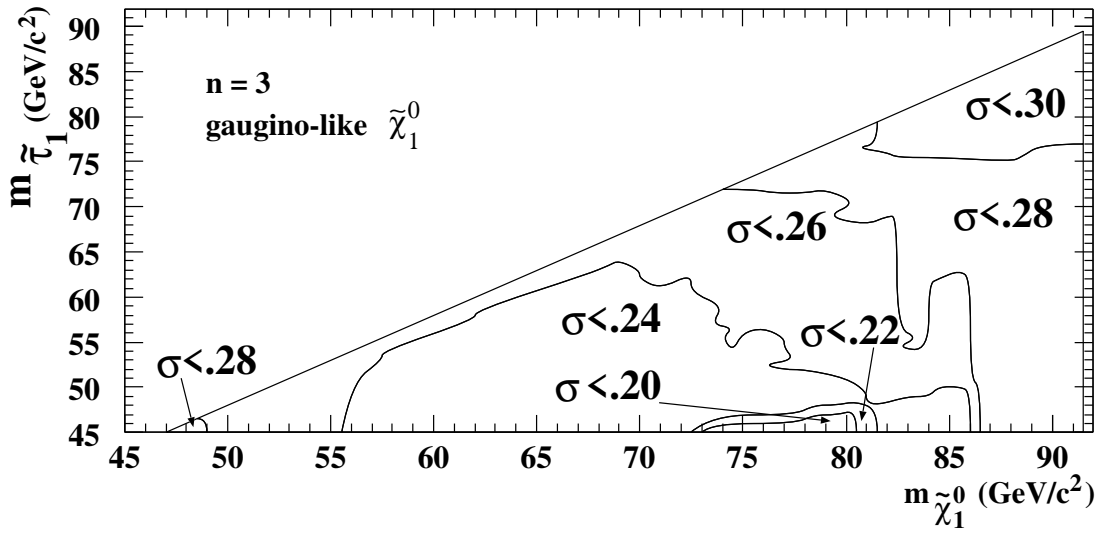

Figure 10: 95% C.L. upper limit of the $\tilde{\chi}_1^0$ pair production cross-section (in picobarn) at $\sqrt{s} = 183$ GeVafter combining the results of the searches at $\sqrt{s} = 161$, 172 and 183 GeV, as a function of $m_{\tilde{\chi}_1^0}$ and $m_{\tilde{\tau}_1}$ for the case $n = 3$ and gaugino-like neutralinos, where n is the number of messenger generations. The diagonal and vertical lines show respectively the limits $m_{\tilde{\chi}_1^0} = m_{\tilde{\tau}} + m_{\tau}$ and $m_{\tilde{\chi}_1^0} = \sqrt{s}/2$.

neutralino is 78 GeV/c^2. The negative-slope dashed area is excluded by the analysis searching for neutralino pair production followed by the decay $\tilde{\chi}_1^0 \to \tilde{G}\gamma$. The point-hatched area is excluded by the direct search for MSSM $\tilde{\tau}_1$ pair production [10], taking into account the possibility of $\tilde{\tau}_L - \tilde{\tau}_R$ mixing [7].

For other cases, lower limits for the mass of the lightest neutralino obtained with this analysis are described in table 5. In the case of $n = 1$ and gaugino-like lightest neutralino, the NLSP is always $\tilde{\chi}_1^0$, and the lower limit is derived from the search for acoplanar photons [11].

n	gaugino-like $\tilde{\chi}_1^0$ (GeV/c^2)	higgsino-like $\tilde{\chi}_1^0$ (GeV/c^2)
1	81.0	71.0
2	78.0	71.0
3	77.0	49.0
4	78.0	45.0

Table 5: The 95% C.L. lower limits on $m_{\tilde{\chi}_1^0}$ for eight different scenarios. When $n = 1$ and the lightest neutralino is gaugino-like, the limit comes from the search for two acoplanar photons.

4.2 Stau pair production

No candidate was observed to pass the selection of the large impact parameter and secondary vertex searches while the total number of background events expected was 0.63 (0.37 on the vertex search and 0.26 on the large impact parameter search). The results of these analyses were combined with those of the stable heavy lepton search described

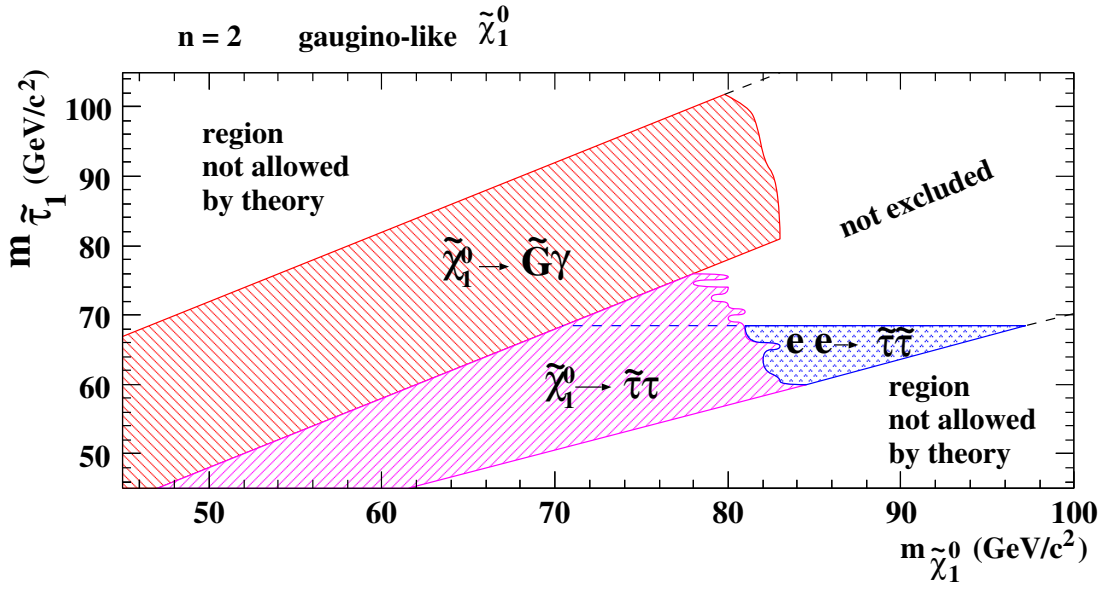

Figure 11: Areas excluded at 95% C.L. for $n = 2$, gaugino-like neutralinos and $m_{\tilde{G}} < 1$ eV in the $m_{\tilde{\chi}_1^0}$ *vs.* $m_{\tilde{\tau}_1}$ plane. The positive-slope dashed area is excluded by this analysis. The negative-slope dashed area is excluded by the search for $\tilde{\chi}_1^0 \to \gamma\tilde{G}$, and the point-hatched area by the direct search for stau pair production in the MSSM framework. The wiggled curve indicating the limit from the search for neutralino pair production, is due to a rapid variation in the 95% C.L. limit on the production cross section.

in [9], which considers $\tilde{\tau}_1$ decays outside the tracking devices ($R > 200$ cm). For very large $\tilde{\tau}_1$ masses, efficiencies around 80% were obtained by the heavy lepton search. Given that an event could be selected both by the vertex search and by the stable heavy lepton search, the correlation was taken into account.

One candidate was observed to pass the small impact parameters search, due to a leading track with $b_1 = 1.3$ mm caused by an interaction with the material of the microvertex detector. A maximum efficiency of around 40% was estimated for this search, and the expected SM background was 1.97 events.

Figure 12 shows the 95% C.L. upper limit on the stau pair production cross-section at $\sqrt{s} = 183$ GeV after combining the results of the searches at $\sqrt{s} = 161$, 172 and 183 GeV with the maximum likelihood ratio method [28]. The results are presented in the ($m_{\tilde{G}}$,$m_{\tilde{\tau}_1}$) plane combining the two impact parameter searches and the vertex analysis. The minimum upper limits achieved for a given $\tilde{\tau}_1$ were around 0.10-0.15 pb depending on $m_{\tilde{G}}$. For 13 eV/c^2 $< m_{\tilde{G}} <$ 150 eV/c^2 and a 70.0 GeV/c^2 $\tilde{\tau}_1$, a 0.15 pb limit was obtained.

The upper limits on the production cross-section were used to exclude $m_{\tilde{\tau}_1}$ values as a function of $m_{\tilde{G}}$ combining all LEP2 energies, assuming conservatively the $\tilde{\tau}_1$ to be right-handed. The vertex analysis allows the exclusion of $\tilde{\tau}_R$ masses between 70.0 and 77.5 GeV/c^2 at 95% C.L. in the range of intermediate gravitino masses (25 to 150 eV/c^2), the stable heavy lepton search covers the high gravitino mass region (over 100 eV/c^2), while the large and small impact parameter searches cover the region of low gravitino masses.

Combining these results with the results of the search for MSSM $\tilde{\tau}_R$, allows the exclusion of stau masses below 68.5 GeV/c^2 irrespective of the gravitino mass. The results are shown in Figure 13, for $\tilde{G}$ larger than 250 eV/c^2 (not shown in the plot) the limit was

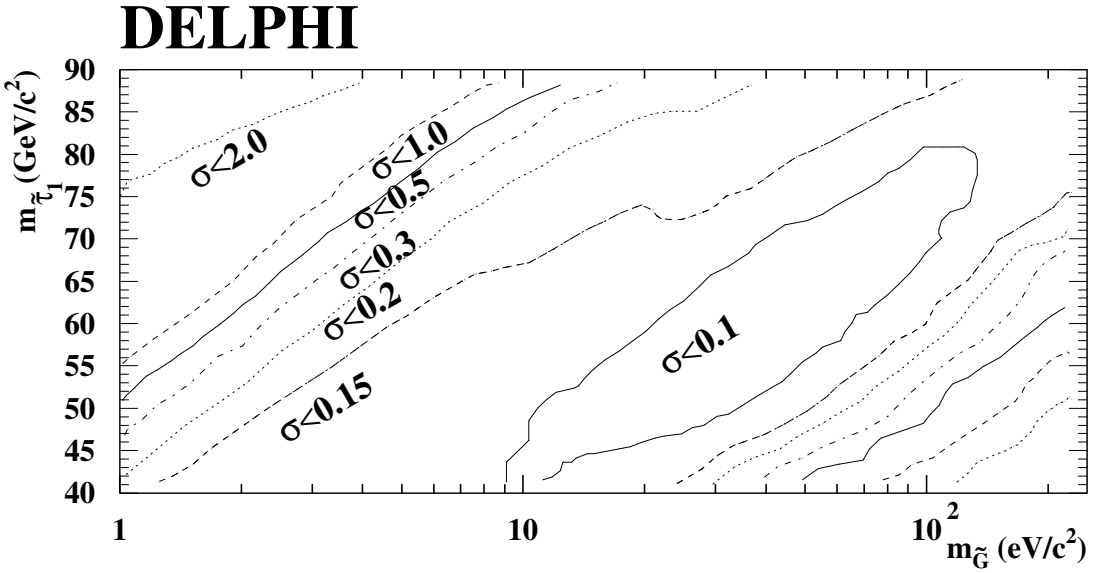

Figure 12: 95% C.L. upper limit of the $e^+e^- \to \tilde{\tau}\tilde{\tau}$ production cross-section (in picobarn) at $\sqrt{s}$ = 183 GeV after combining the results of the searches at $\sqrt{s}$ = 161, 172 and 183 GeV. Results are shown in the ($m_{\tilde{G}}$,$m_{\tilde{\tau}_1}$) plane. Searches for events containing charged tracks with small impact parameter, large impact parameter or vertices are used.

80.0 GeV/c^2 obtained from the stable heavy lepton search [9]. Following [4] as in section 4.1, figure 14 shows the 95% C.L. excluded areas for the case of $n = 2$, gaugino-like neutralinos and $m_{\tilde{G}} = 40$ eV/c^2 in the $m_{\tilde{\chi}^0_1}$ *vs.* $m_{\tilde{\tau}_1}$ plane. The negative-slope dashed area is excluded by the analysis searching for neutralino pair production followed by the decay $\tilde{\chi}^0_1 \to \tilde{G}\gamma$. The point-hatched area is excluded by this search taking into account the possibility of $\tilde{\tau}_L - \tilde{\tau}_R$ mixing [7]. The resulting 95% C.L. lower limit on the mass of the lightest neutralino is 62 GeV/c^2, and that for the stau 60 GeV/c^2, from the neutralino pair production search.

By comparing figures 11 and 14 it can be seen that the exclusion power of isolated photon searches decreases as the mass of the gravitino increases. It can also be seen that the area excluded by the stau pair production searches increases with $m_{\tilde{G}}$.

5 Summary

Lightest neutralino and stau pair production were searched for in the context of light gravitino scenarios. It was assumed that the $\tilde{\tau}_1$ is the NLSP and that the $\tilde{\chi}^0_1$ is the NNLSP. Both searches were used in order to explore the ($m_{\tilde{\chi}^0_1}, m_{\tilde{\tau}_1}$) plane in different domains of the gravitino mass.

The search for neutralino pair production produced two candidate events to be compared to 0.77±0.16 events expected from the SM background for the samples ranging from $\sqrt{s}$ = 161 GeV up to 183 GeV. An upper limit on the corresponding production cross-section between 0.2 and 0.3 pb was set at 95% C.L. in the kinematically allowed region.

The search for the pair production of long lived staus produced one candidate for the small impact parameter method and none for the large impact parameter and vertex

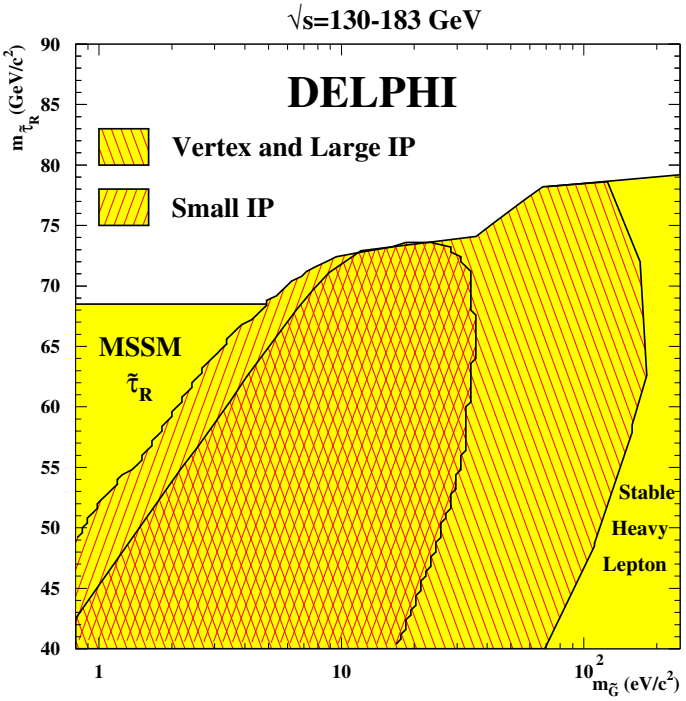

Figure 13: Exclusion region in the ($m_{\tilde{G}}$,$m_{\tilde{\tau}_R}$) plane at 95% C.L. for the present analysis combined with the stable heavy lepton search and the MSSM $\tilde{\tau}_R$ search, using all LEP-2 data. The positive-slope hatched area shows the region excluded by the small impact parameter search. The negative-slope hatched area shows the region excluded by the combination of the large impact parameter and secondary vertex searches.

methods, whereas totals of $2.68^{+0.84}_{-0.31}$ and $0.63^{+0.55}_{-0.12}$ events were expected from the simulated SM background, respectively. An upper limit on the stau pair production cross-section was set as a function of its mass and that of the gravitino, between 0.1 and 2 pb at 95% C.L. in the kinematically allowed region. This result, together with the search for staus within the MSSM framework and stable stau production, allow the DELPHI collaboration to set the lower limit on the mass of the $\tilde{\tau}_R$ at 68.5 GeV/c^2 at 95% C.L..

Acknowledgements

We would like to thank S. Nandi, K. Cheung and C. Wagner for very useful discussions in theoretical matters. We are greatly indebted to our technical collaborators building and operating the DELPHI detector and to the members of the CERN-SL Division for the excellent performance of the LEP collider.
We are also grateful to the technical and engineering staffs in our laboratories and we acknowledge the support of
Austrian Federal Ministry of Science, Research and Arts,
FNRS–FWO, Belgium,
FINEP, CNPq, CAPES, FUJB and FAPERJ, Brazil,
Czech Ministry of Industry and Trade, GA CR 202/96/0450 and GA AVCR A1010521,
Danish Natural Research Council,
Commission of the European Communities (DG XII),

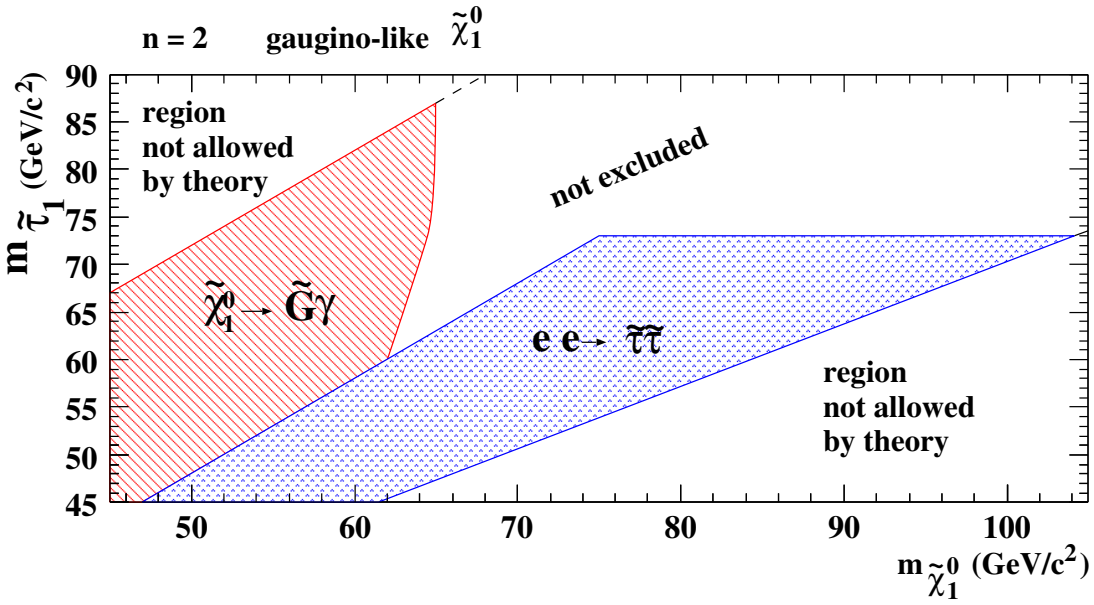

Figure 14: Areas excluded at the 95% C.L. for $n = 2$, gaugino-like neutralinos and a 40 eV/c^2 gravitino in the $m_{\tilde{\chi}_1^0}$ *vs.* $m_{\tilde{\tau}_1}$ plane. The negative-slope dashed area is excluded by the search for $\tilde{\chi}_1^0 \to \gamma\tilde{G}$ and the point-hatched area by this analysis.

Direction des Sciences de la Matière, CEA, France,
Bundesministerium für Bildung, Wissenschaft, Forschung und Technologie, Germany,
General Secretariat for Research and Technology, Greece,
National Science Foundation (NWO) and Foundation for Research on Matter (FOM), The Netherlands,
Norwegian Research Council,
State Committee for Scientific Research, Poland, 2P03B00108, 2P03B03311 and 628/E–78–SPUB–P03–023/97,
JNICT–Junta Nacional de Investigação Científica e Tecnológica, Portugal,
Vedecka grantova agentura MS SR, Slovakia, Nr. 95/5195/134,
Ministry of Science and Technology of the Republic of Slovenia,
CICYT, Spain, AEN96–1661 and AEN96-1681,
The Swedish Natural Science Research Council,
Particle Physics and Astronomy Research Council, UK,
Department of Energy, USA, DE–FG02–94ER40817.

References

[1] M. Dine, W Fischler and M. Srednicki, Nucl. Phys. **B189** (1981) 575;
S. Dimopoulos and S. Raby, Nucl. Phys. **B192** (1981) 353;
M. Dine and W. Fischler, Phys. Lett. **B110** (1982) 227;
M. Dine and M. Srednicki, Nucl. Phys. **B202** (1982) 238;
L. Alvarez-Gaumé, M. Claudson and M. Wise, Nucl. Phys. **B207** (1982) 96;
C. Nappi and B. Ovrut, Phys. Lett. **B113** (1982) 175.

[2] M. Dine and W. Fischler, Nucl. Phys. **B204** (1982) 346;
S. Dimopoulos and S. Raby, Nucl. Phys. **B219** (1983) 479.

[3] J. A. Bagger, K. Matchev, D. M. Pierce and R. Zhang, Phys. Rev. **D55** (1997) 3188.

[4] D.A. Dicus, B. Dutta and S. Nandi, Phys. Rev. **D56** (1997) 5748;
D.A. Dicus, B. Dutta and S. Nandi, Phys. Rev. Lett. **78** (1997) 3055.

[5] F. Borzumati, *On the Minimal Messenger Model*, hep-ph/9702307.

[6] G.F. Giudice and R. Rattazzi, *Theories with Gauge-Mediated Supersymmetry Breaking*, hep-ph/9801271, submitted to Phys. Rev. D.

[7] A. Bartl *et. al.*, Z. Phys. **C73** (1997) 469.

[8] S. Dimopoulos, M. Dine, S. Raby, S. Thomas and J.D. Wells, Nucl. Phys. Proc. Suppl. **52A** (1997) 38.

[9] DELPHI Collaboration, P. Abreu *et al.*, Phys. Lett. **B396** (1997) 315;
DELPHI Collaboration, P. Abreu *et al.*, CERN-EP/98-171, submitted to E. Phys. J. C.

[10] DELPHI Collaboration, W. Adam *et. al.*, *Search for Sfermions at* $\sqrt{s}$ *= 130 to 183 GeV*, contribution # 204 to ICHEP'98, XXIX Intenational Conference on High Energy Physics, Vancouver.

[11] DELPHI Collaboration, P. Abreu et al, CERN-EP/98-142, accepted by E. Phys. J. C.

[12] DELPHI Collaboration, P. Abreu et al, CERN-EP/98-116, accepted by E. Phys. J. C.

[13] DELPHI Collaboration, P. Aarnio et al., Nucl. Instr. and Meth. **303** (1991) 233.

[14] DELPHI Collaboration, P. Abreu et al., Nucl. Instr. and Meth. **378** (1996) 57.

[15] T. Sjöstrand, Comp. Phys. Comm. **39** (1986) 347;
T. Sjöstrand, `PYTHIA 5.6` *and* `JETSET 7.3`, CERN-TH/6488-92.

[16] DELPHI Collaboration, P. Abreu *et al.*, Z. Phys. **C73** (1996) 11.

[17] SUSYGEN 2.12, S. Katsanevas and S. Melachroinos in *Physics at LEP2*, CERN 96-01, Vol. 2, p. 328 and http://lyohp5.in2p3.fr/delphi/katsan/susygen.html .

[18] J.E. Campagne and R. Zitoun, Z. Phys. **C43** (1989) 469.

[19] S. Jadach and Z. Was, Comp. Phys. Comm. **79** (1994) 503.

[20] F.A. Berends, R. Kleiss and W. Hollik, Nucl. Phys. **B304** (1988) 712.

[21] F.A. Berends, R. Pittau and R. Kleiss, Comp. Phys. Comm. **85** (1995) 437.

[22] S. Nova, A. Olshevski and T. Todorov, *A Monte Carlo event generator for two photon physics*, DELPHI note 90-35 (1990).

[23] F.A. Berends, P.H. Daverveldt, R. Kleiss, Comp. Phys. Comm. **40** (1986) 271, Comp. Phys. Comm. **40** (1986) 285, Comp. Phys. Comm. **40** (1986) 309.

[24] DELPHI Collaboration, P. Abreu *et al.*, E. Phys. J. **C2** (1998) 1.

[25] S. Catani, Phys. Lett. **B269** (1991) 432.

[26] DELPHI Collaboration, P. Abreu *et al.*, Zeit. Phys. **C74** (1997) 57.

[27] P. Billoir and S. Qian, Nucl. Instr. and Meth. **311** (1992) 139.

[28] A.L. Read, *Optimal statistical analysis of search results based on the likelihood ratio and its application to the search for the MSM Higgs boson at* $\sqrt{s}$ *= 161 and 172 GeV*, DELPHI 97-158 PHYS 737 (1997) and references therein.